Crystallization processes in bicomponent thin film depositions: towards a realistic kinetic Monte Carlo simulation

D. Martínez-Martínez[1,], C. Herdes[2], Lourdes F. Vega[3]*

[1]Center of Physics of the University of Minho, Campus de Azurem, 4800-058 Guimaraes, Portugal.

[2]Department of Chemical Engineering, University of Bath, Claverton Down, Bath, Somerset BA2 7AY, United Kingdom.

[3]Gas Research Center and Chemical Engineering Department. Khalifa University of Science and Technology. The Petroleum Institute. P.O. Box 2533. Abu Dhabi. United Arabs Emirates.

*corresponding author e-mail: diegus.m2@gmail.com

Abstract

The kinetic Monte Carlo (KMC) method is a powerful and simple tool to simulate the growth of thin films by deposition. However, one of its major drawbacks is the artificial order induced by the use of regular lattices. An algorithm that mimics the crystallization processes in bi-component thin film depositions via a novel KMC approach is presented in this work. This new algorithm, named GEM-CA (Geometrical Energy Modification-Crystallization Algorithm), modifies the hopping energy barrier depending on the geometrical configuration of the atoms surrounding one particular position.

The novel approach allows obtaining amorphous, crystalline and mixed structures (i.e. nanocomposites), depending solely on the synthesis parameters. In addition, we have developed a method for the analysis of deposited structures based on their degree of order. The influence of different deposition parameters such as temperature or composition is discussed in detail. GEM-CA reproduces experimentally observed trends of bi-component film deposition.

Keywords: kinetic Monte Carlo, thin film deposition, crystallization, polycrystal, nanocomposite.

1. Introduction

The properties of most common substrates can be modified by coating deposition. In particular, thin film technology is commonly used to improve some of the optical, chemical, mechanical, tribological and other properties of some substrates for specific applications [1]. Coating technology involves several different techniques, such as physical vapour deposition (PVD), chemical vapour deposition (CVD), thermal reduction, electrochemical methods, etc. [1]. Among them, PVD, which consist on the atom evaporation from a source and its deposition on the substrate surface, is widely used.

Nowadays, experimental results are interpreted in many cases with the help of computer simulations. In fact, simulation techniques are becoming standard tools to investigate and advance the understanding of the synthesis process and the properties of materials. They are versatile and relatively cheap in comparison to the laboratory techniques; in addition, they provide information that is not accessible through direct experimentation, and allow studying the individual effect of synthesis parameters interconnected in real processes. There is a large variety of simulation methods for coating deposition, ranging from very accurate models, derived from quantum-mechanical calculations, to reactor-scale simulations [2]. In general, the former methods can reach very high levels of detail and complexity, at the expenses of reducing the time and space scales of the analysis, and vice-versa [2].

Among the different possibilities, the kinetic Monte Carlo (KMC) method has been widely used to study PVD, as it represents a balance between modest computational time (compared to quantum-mechanical calculations) and good description of the system. KMC divides PVD into two subsequent processes: i) atom deposition over the substrate, and ii) diffusion of atoms. In some cases, re-evaporation of atoms from the surface is also considered [3]. The deposition is normally simulated as a ballistic process, which can be approached with different degrees of detail, including the possibility of having a rotary system [4], the impact energy of ions and the angle of bombardment [5]. Diffusion is simulated by a model in which atoms make short jumps over a regular lattice (hopping model). Atoms on the surface jump from one site to another, by overcoming a certain energy barrier. There are several approaches found in the

literature to calculate such barriers (see e.g. refs. [6–8]). A convenient choice is obtaining the values of these barriers from molecular dynamics, and simulating the growth with KMC [9,10]. The lattice geometry (cubic [7] or hexagonal [4]) and dimensions [5] (bi-dimensional or tri-dimensional) vary depending on the problem under study.

Besides the obvious advantages of KMC (simplicity, flexibility and wide scales of time and length reachable), the main problem it faces for simulating PVD is the use of a regular lattice with fixed positions. That lattice imposes an artificial degree of order over atoms deposited on the surface, finally resulting in an ordered system (monocrystal), while different types of structures (e.g. amorphous, polycrystal, etc.) are observed in real processes. For instance, Figure 1 shows high-resolution transmission electron microscopy of a polycrystalline TiC (Fig. 1a) and a nanocomposite formed by TiC nanoparticles embedded in an a-C matrix (Figure 1b) prepared by co-sputtering [11]. It is not possible to obtain these structures by conventional KMC since ordered and disordered structures are indistinguishable with the classical KMC approach.

Some attempts to overcome this difficulty have been already made by some authors. For instance, Wang and Levine [12] introduced artificial grain boundaries on the system, and Bruschi [13] and Ono [14] divided the surface into misoriented cells. However, in these cases, the polycrystal nature is introduced in the simulation instead of being a result of it, which biases the obtained results.

The aim of the present work is to provide a new KMC simulation algorithm that allows obtaining structures similar to those observed in Figure 1, i.e. to study the formation and growth of polycrystals or nanocomposites, as well as the influence of several parameters in these processes. For this purpose, a novel crystallization algorithm that modifies the energy-hopping barrier depending on spatial arrangements has been developed, the Geometrical Energy Modification-Crystallization Algorithm (hereafter referred as GEM-CA). The use of two different atoms during the deposition allows the introduction of occupational order and disorder, even in the presence of a regular substrate lattice.

2. Description of the model

2.1. Background

The model presented here is based on the work of Helin et al. [8] and Tan et al. [15], being an extension of them. The coating growth is a process consisting of a random vertical ballistic deposition of atoms and subsequent diffusion on the surface. The atoms are deposited on a bi-dimensional square lattice (same number of sites in vertical and horizontal directions) with a compact hexagonal packaging, chosen due to its higher symmetry. The deposition process is characterized by the deposition rate (monolayers/s) and time (s); the percentage of surface coverage and the time between depositions of atoms are inferred from these values.

The diffusion is controlled by atoms hopping over the surface, using periodic boundary conditions. The time consumed by a diffusion process (t_{diff}) depends on its rate (ν_{diff}):

$$t_{diff} = \frac{1}{\nu_{diff}} \qquad [1]$$

The diffusion rate is calculated by an Arrhenius-type expression:

$$\nu_{diff} = \frac{2kT}{h}\exp\left(-\frac{E_B}{kT}\right) \qquad [2]$$

where k and h are the Boltzmann´s and Planck´s constants, respectively, T is the absolute temperature and E_B is the activation barrier. The latter term is composed of different contributions:

$$E_B = E_S + \beta E_L + (\Delta\alpha)E_D + \Delta E_N \qquad [3]$$

where Δ is an operator which represents the difference between the final and initial states, E_S is the energy of interaction of the atoms with the substrate (in other words, an energy barrier always present in a diffusion event). E_D is the substrate defect energy, which has to be taken into account for atoms next to substrate defects, and α is the number of defects next to a given atom. These defects are often introduced in KMC, and serve as seeds for grain nucleation.

The number of substrate defects on the surface is introduced as an input variable, and they are distributed randomly over the surface at the beginning of the calculations. E_L is the "ladder energy", an energy barrier that accounts for the presence of obstacles (atoms or defects) along the diffusion path (see Figure 2a). β represents the number of these obstacles, with possible values 0, 1 or 2. E_N is the energy of the neighbour atoms, and it is calculated by a Morse potential, at the beginning and at the end of the diffusion event. According to [8,14], E_N is calculated considering Next Neighbours (NN) and Next Nearest Neighbours (NNN) atoms, allowing 18 neighbours per position (see Figure 1b). For a site *i* on the lattice the expression is as follows:

$$E_N(i) = \sum_{j=1}^{NN,\,NNN} E_{ji}\,,\; E_{ji} = V_0\left[\exp\left(-2a\frac{r_{ij}-r_0}{r_0}\right) - 2\exp\left(-a\frac{r_{ij}-r_0}{r_0}\right)\right] \qquad [4]$$

where V_0 is the energy interaction between NN, a is a constant that controls the width of the curve, and r_0 and r_{ij} are the distance between NN and i and j atoms, respectively, expressed in atomic units. The values of E_S, E_B, E_L, V_0 and a have been taken from the work of Helin et al. [8] and Tan et al. [15], following the work of Voter [16]. They are summarized in Table 1 for completeness. Since only NN and NNN are checked, just three values of r_{ij} and E_{ij} are possible, as indicated in Figure 2b. Therefore, Eq. 4 can be reduced to:

$$E_N = n_{NN}E_{NN} + n_{NNN1}E_{NNN1} + n_{NNN2}E_{NNN2} \qquad [5]$$

where n_{NN}, n_{NNN1}, and n_{NNN2} are the number of NN, NNN1 and NNN2 occupied positions respectively (see Figure 2b). Then, by substituting E_N from Eq. (5) in Eq. (3), we obtain:

$$E_B = E_S + \beta E_L + (\Delta\alpha)E_D + \Delta n_{NN}E_{NN} + \Delta n_{NNN1}E_{NNN1} + \Delta n_{NNN2}E_{NNN2} \qquad [6]$$

The algorithm follows the next sequence of events (a detailed scheme is included in the Supplementary Material):

1. Lattice preparation and random distribution of defects.
2. Random deposition of one atom on a free site of the surface. Diffusion takes place until the deposition of a new atom is enforced, according to the simulation input parameters. The time interval between the depositions of two

consecutive atoms is the diffusion time, inversely dependent on the deposition rate.

3. Calculation of the rate of all the possible diffusion events from any occupied position to any empty NN. Notice that diffusion to NNN is not allowed. All the possible events are recorded in a matrix that includes the initial and final sites, the individual diffusion rate and the accumulated rate (sum of all the individual diffusion rates calculated after the selection of the latest diffusion process). The accumulated rate will become the total rate when the last diffusion process is calculated for a certain configuration.
4. Random selection of a number between 0 and 1. This number is multiplied by the total rate. The event with higher accumulated rate smaller than the result of this multiplication is the selected event. The time consumed by the selected diffusion is calculated using Eq. 1.
5. The lattice occupation is updated, and the time consumed by the event is subtracted from the total diffusion time. More diffusion events are carried out in sequence until the total diffusion time is exhausted.
6. Then, a new atom will be deposited, and the cycle (from 2 to 5) will be repeated again. It is worth mentioning that, typically, the last diffusion event of a given cycle will last longer than the remaining total diffusion time before a new atom is deposited. Therefore, there would be some 'diffusion time debt (dtd)' that should be considered for the next diffusion cycle after atom deposition. However, such dtd is not discounted in the next cycle. This can be interpreted like an overlapping of diffusion events in time. This ensures that at least one diffusion event per deposited atom occurs, allowing the time to be reset after the deposition of an atom in the surface.
7. The calculations finish when all the atoms are deposited.

2.2. Model modification for crystallization (the GEM-CA)

In the present work, two different types of atoms are used for the deposition procedure, with the composition set as an input variable. When an atom is deposited, its nature (A or B) is randomly selected and compared with the composition, e.g. if the composition is 25% of A, then a random number between 0 and 1 is selected and compared to 0.25. If the random number is

smaller than 0.25, an A atom is deposited onto the substrate, otherwise, a B atom is selected. However, A and B are controlled by the same set of parameters summarized in Table 1, ad hoc, to study the influence of GEM-CA in a situation of perfect symmetry; both A and B atoms behave the same, and the A-A, B-B and A-B interactions are equal, except when GEM-CA is active.

A crystal is a structure in which spatial order is present over a long range. This means that the stability of an atom is higher if it occupies a specific position on a crystal. Therefore, we have introduced this differential behaviour in the energy calculation (a coarse approach to lattice energy). To do this, the NN of all the occupied positions on the surface lattice are evaluated; this allows calculating a parameter (*P*) for all the sites on the surface, which represents which kind of atom (A or B) would be more stable in each position, and the degree of additional (de)stabilization that would gain if it diffuses there. The initial value of *P* is zero for all positions. If the environment of the atom is in agreement with any of the geometrical configurations detailed in Figure 3a (which will be described in detail afterwards), then some of the *P* values of the NN sites are increased by +1 if the preferred atom in that site is A, and decreased by -1 if the preferred atom is of type B. Therefore, at the end of the evaluation, the value of *P* for all the sites is between -6 and +6. The value of +6 represents an A atom which is surrounded by six atoms in a perfect crystal geometry. To reflect this geometrical influence, a new term is added to Eq. (6), which changes to:

$$E_B = E_S + \beta E_L + (\Delta\alpha)E_D + \Delta n_{NN} E_{NN} + \Delta n_{NNN1} E_{NNN1} + \Delta n_{NNN2} E_{NNN2} + z(\Delta P)cE_{NN} \quad [7]$$

where *c* is an input parameter of the program representing the energy benefit of forming an ordered structure (if *c*=0 no benefit would be given); *z* is another parameter that depends on the nature of the diffusing atom (z equals to +1 for atoms of type A and to -1 for atoms of type B).

Figure 3 compares two cases in which a B atom may diffuse from a position with no NN to a position with three NN. In Figure 3b, the atom will diffuse to a position without surrounding order, while in Figure 3c the atom will diffuse to a position with surrounding order (diagonal stacking of A and B planes). In this particular example, the hopping energy barrier is smaller for case (c) than in case (b), although the destination site has the same number of neighbours (NN

and NNN) in both cases. In short, despite the same number and type of neighbours, the diffusion will be preferred in the second case because the atom will be forming part of a crystalline structure after the diffusion jump.

It is worth mentioning that the bonus parameter *P* is only calculated when the central atom has at least one atom in NN which is different than itself (hereafter called "rule of Different NN, DNN rule"). This is necessary to avoid the uncontrolled growth of individual crystal planes, which is also illustrated with an example in Figure 3. In Figure 3d, the value of parameter *P* is shown for unoccupied positions before the diffusion of atom A. The situation after the diffusion event without applying the "DNN rule" is shown in Figure 3e; the new A atom (in red) would give additional stabilization to its NN positions, and therefore the plane formed by A atoms can continue growing without need of the rest of crystal to follow. In contrast, Figure 3f shows the situation after the diffusion event applying the "DNN rule". In this case, the new A atom is not allowed to give bonuses for growing, so the plane growth is delayed until an atom different to itself arrives at the NN site.

These geometrical energetic bonuses are assigned only in few geometrical cases (see Figure 3a, and a more detailed casuistry in the Supplementary Material). In provided examples, it is considered that the atom under study (central atom) is of type A; the situations would be the opposite in case of the central atom would be of type B. The nomenclature n_{NNA} and n_{NNB} refers to the number of sites in NN occupied by atoms of A and B nature, respectively. Of course, if the central atom has no occupied NN sites (n_{NN}=0), then no bonuses are assigned to any of the NN positions. The same happens in case of no NN site occupied by an atom different from the central (n_{NNB}=0 in Fig. 3a) due to the abovementioned DNN rule. In case of having NN sites occupied by atoms of the same type than the central one (n_{NNA}=1, 2, 3, 4 in Fig. 3a), energetic bonuses are assigned in order to promote the growth of the crystalline planes (*plane-growth configurations*). The idea is that, in case that the central atom is involved in a plane whose growing direction is clear, then the energetic benefits will favour such geometry. However, it could happen that the central atom has two NN atoms like itself (n_{NNA}=2 in Fig. 3a) in contact between them (*cumulus configuration*). This case can be achieved by a diffusion process to a less-stable

site, or due to a direct deposition of an atom in a less-stable site (this event is almost impossible in a real deposition process, but it becomes significant in the simulations due to the limited number of positions available on the lattice). In case of cumulus configuration illustrated in Fig. 3a, there are two possibilities for the plane formed by A atoms to grow, and hence both possibilities are energetically favoured. When an A atom occupies one of these sites, the geometry will evolve to a *plane-growth configuration* one, and the other possible growing direction will be energetically penalized. Finally, in the cases of a central atom with no NN sites occupied by atoms of the same type (n_{NNA}=0 in Figure 3a, *Induced-plane configurations*) the geometry has to allow the possibility of growth of a crystalline plane involving the central atom. This means that at least two empty sites must be in opposed positions. In the first two cases, where at least two atoms different to the central one are present ($2 \leq n_{NNB} \leq 4$ in Fig. 3a), the choice of the position of these empty sites is clear, and therefore all bonuses to the six NN's can be given. In contrast, if two possibilities of the plane growth are present ($1 \leq n_{NNB} \leq 2$, the last case in Fig. 3a), then bonuses are only assigned to positions that can be occupied by atoms different from the central atom (type B in Fig. 3a).

The final orientation of the crystal will be selected when one of the NN empty sites would be filled; thus, if an atom different to the central one arrives (B in Fig. 3a), the configuration would change to one of the *induced-plane configurations* mentioned before. In contrast, if an atom equal to the central one arrives (A In Fig. 3a), the configuration is transformed into the first *plane-growth configuration*. In any of the cases, the growth of the crystal will continue.

3. Results and discussion

3.1. Effect of GEM-CA and symmetry analysis.

Table 2 summarizes the values of different deposition parameters kept constant (lattice size, number of defects, deposition rate and deposition time) and the variable ranges for the deposition parameters studied in this work (parameter *c*, composition and temperature). Constant values are marked in **bold** when another deposition parameter is varied.

Figure 4 shows pictures of two films deposited under the same conditions, with the only difference of inactivation (c=0) or activation (c=1) of GEM-CA. Both cases are depicted in Figure 4, with surface coverages of 50% (Figs. 4a, c) and 100% (Figs. 4b, d). A clear difference can be observed between them; when GEM-CA is inactive (c=0), large disordered islands grow until the surface is covered. In contrast, the activation of GEM-CA (c=1) leads to the formation of smaller ordered grains that will grow until the whole substrate is filled. This result is of clear relevance to the present study, since it demonstrates that this approach is a good choice to simulate an amorphous coating over a completely regular lattice. Nevertheless, and strictly speaking, an amorphous phase composed exclusively of one type of atoms will be also well-ordered, due to the influence of the underlying lattice (i.e. the location of all the atoms will be regular). However, this situation can be also considered in our simulations as 'disordered' (or 'amorphous') in the sense that such arrangement does not present A-B occupational order (i.e. A-B-A-B crystalline planes). In this sense, GEM-CA allows distinguishing between both structures (crystalline and amorphous) even in the situation of complete surface coverage, which is not achievable in other circumstances (for instance, if only one type of atom or no bias towards the formation of ordered A-B structures are considered).

It is worth mentioning that, in spite of using GEM-CA, some agglomerates of A and B are formed even at the beginning of the deposition. This is a normal effect, because, although GEM-CA promotes the formation of A-B crystals, the attractive forces between atoms of the same type (without forming crystals) are not eliminated; in other words, the formation of an AB grain *stabilizes more* than the formation of AA and BB agglomerates, but these latter ones are *more stable* alternatives than isolated A or B atoms. In order words, atoms will always tend to form aggregates, although ordered AB arrangements will be preferred, if possible.

The deposited structures can be further analysed by considering the symmetry and types of atoms in NN to each site. Such analysis allows re-plotting the images of the left column of Figure 4 towards the images included in the central part of Figure 4 (see Table 3 for definitions and explanation of the colour code). The atoms belonging to a grain can be classified from higher to lower quality,

which it is generally correlated to the proximity to the centre of the grain. *Crystalline* atoms are those surrounded by 6 NN atoms in well-ordered configuration (i.e. one crystalline atom that has P=±6). These atoms can be sub-divided into *internal* if these six NN are also crystalline, and *external* if at least one of these NN atoms is not crystalline. Those atoms in NN to a crystalline external that are not crystalline are labelled as *boundary* atoms, i.e. atoms that are needed to complete the surrounding of a crystalline external. In special cases, boundary atoms can be re-classified as *twin* atoms or *triple junctures*, if they belong to two or three different grains, respectively. In this latter case, the triple juncture is the conjunction of three twins, very infrequent in the simulations (observed not more than three times in 10^4 atoms in a given simulation). Finally, *growing* atoms are defined as those that are in contact with boundary atoms (or other growing) that show the same symmetry than the grain that they are connected to, except for the fact that they are not totally surrounded by six NN (i.e. they are not crystalline because there is at least one position empty).

It is worth mentioning that, under these definitions, the smallest grain is formed by seven atoms (one crystalline external surrounded by six boundaries). In other words, at least one atom has to be surrounded by six well-ordered NN to consider the formation of a grain. Therefore, if a group of atoms is well-ordered in layers, but none of them complies with the previous constrain, none of them will be considered as crystalline.

In addition to crystalline atoms, two additional types of positions can be identified: *antisite defects* and *vacancies.* These are positions within a grain that are occupied by a 'wrong' atom or an empty site, respectively. In both cases, they appear surrounded by boundary atoms. In this analysis, these positions are only considered when they are isolated, i.e. two defects or vacancies as NN (or their combinations) are not considered. Finally, atoms not belonging to any of the defined cases are considered as *amorphous*.

Examples of all these cases can be observed in the central column of Figure 4, which can be easily correlated with the original deposition (left column). It can be seen that very small 'grains' can be also detected in the amorphous film, just

by coincidence, which is a consequence of the presence of an ordered lattice as substrate.

As a further step we have also analysed the connection of these individual atoms to form *grains*. This calculation is based on the orientation of the NN's of all the different crystalline atoms described before (internal, external, boundary and growing). Since for the hexagonal lattice there are three possible orientations (horizontal and two diagonals), and two different possibilities for each orientation (in a grain, the A atoms may be located in the even or odd rows of the lattice, and vice versa for the B atoms), six types of grains may exist, which are represented with six different colours in the images included in the right column of Figure 4. It is important to clarify that the three possible orientations of crystals obtained by the simulations are actually imposed by the lattice geometry; however, the size and number of crystals are a result of the simulations, and depend on synthesis parameters, instead of being introduced as input parameters.

It should be noticed that twin and triple juncture atoms are not considered to belong to any particular grain, and therefore they are explicitly represented in these images (right column) as in the previous ones (central column). The same applies for defects and vacancies, which are also included with the same colour code as in the previous pictures. Atoms belonging to the amorphous phase are not shown in these representations to avoid confusion with the grains.

The analyses carried out on the deposited films allow the quantification of different parameters that are very useful for the statistical evaluation of the film growth, e.g., percentage of deposited atoms being crystalline, average grain size, the average ratio of external/internal atoms in the grains, the average stoichiometry of the grains, or the average composition of the amorphous phase. Such parameters will be employed to characterize and compare quantitatively the different depositions in the next subsections.

3.2. Influence of simulation parameters.

3.2.1. Influence of parameter c

The influence of three deposition parameters has been studied in this work (see Table 2): the *c* parameter, the chemical composition of the film, and the deposition temperature (see Figure 5). Three different simulations have been performed for each condition. The *c* parameter controls the energetic biasing that the atoms suffer towards crystallization (cf. Eq. 7), and therefore its choice is very relevant. Simulations performed at T=500 K and compositions of 25 and 50% were used to evaluate the influence of this parameter on the statistical parameters defined before, as depicted in the left column of Figure 5.

Fig. 5a shows the average number of diffusions per deposited atom. For values of *c*=0.25, the number of diffusions decreases for both systems in similar amounts. At this value of *c*, the film growth (not shown) is similar to what it is depicted Figure 4a (i.e. large islands, instead of the ordered crystals observed in Fig. 4c). However, for *c*=0.25, more small grains are present within each large island, which probably hinders the diffusion events. Further increase of *c* causes the number of diffusions to grow again, and it induces the separation of both compositions, with higher number of diffusions observed for 50%. This is because the GEM-CA algorithm reduces the diffusion energy, leading to lower diffusion times. For a composition of 50%, there are more chances to form more and larger grains, the diffusion time will be lower due to GEM-CA, and therefore the number of diffusion events will be higher.

Figure 5b shows the final crystalline coverage (CC) depending on the value of *c*. The experimental data have been fitted to an exponential equation with the form:

$$CC\ (\%) = CC_0 + \Delta CC\left(1 - exp\left(-\frac{c}{K}\right)\right) \qquad [8]$$

where CC_0 and ΔCC represent the initial value (CC at *c*=0) and range of variation of CC, respectively. The constant *K* indicates the shape of the exponential curve, i.e. how quick steady state is reached. It can be seen in Fig. 5b that the steady state of both curves (CC_0+ΔCC) is achieved for CC's of 49% and 93% for compositions of 25 and 50%, respectively. Those values are very

close to the theoretical compositional limits (50% and 100%, respectively). It is worth mentioning that the values of CC_0 are not zero; in contrast, they are as high as 11.8 and 25.7 for compositions of 25 and 50%, respectively. These values represent the crystalline coverage by 'random grains' that appear when GEM-CA is disconnected (c=0). Finally, the value of K is double for a composition of 50% (0.69 vs. 0.35). This means that the 'saturation' is reached at lower values of c for the composition of 50%. In fact, this is a relevant reason to set the value of c=1 for new simulations. A further increase of c causes no improvement in crystallization (i.e. not more crystalline atoms), but the grain sizes are dramatically increased (by a factor of 2 from c=1 to c=3), as it can be appreciated in Fig. 5c. Therefore, higher values of c only promote grain growth at the expenses of nucleation. Such process may be problematic considering the size of the simulation cell and the periodic boundary conditions. Therefore, the value of c=1 is preferred. With a composition of 25%, the growth of the grain size is more modest, since the presence of the amorphous phase serves as a barrier for uncontrolled grain growth (cf. much lower number of diffusions in Fig 5a).

Figure 5d shows the average ratio of external-to-internal crystalline atoms. The maximum value of this ratio is six in a hexagonal planar lattice. For values of c=0, both compositions are close to this value (ratio 4.8 for a composition of 25%), in good agreement with the low value of average grain size observed for c=0 in Fig. 5c (ca. 8.4 atoms, being the minimum 7). Both compositions show a decreasing trend for larger values of c, in agreement with the increased grain sizes. The film with a composition of 50% shows lower values, reaching a ratio of 0.33 for c=3, which means three internal crystalline atoms per external crystalline one.

The grain stoichiometry and composition of the amorphous phase are depicted in Figure 5e and f. For simulations carried out with a composition of 50%, both values are around 1% and 50%, respectively. The trend in Fig 5f is noisier because the quantity of amorphous phase is quite low (cf. Fig 1b). In contrast, at a composition of 25%, the grains are enriched up to a stoichiometry around 1.2-1.25, richer in the most abundant atom. Such value seems to be quite constant regardless of grain size or crystalline coverage. In addition, the

composition of the amorphous phase shows a decreasing trend from ca. 22% to 7%. The composition of the amorphous matrix is expected to be very pure (i.e very low concentration of the atom in lower proportion), since the less abundant atoms would be 'better employed' to form energetically-favourable grains. However, the amorphous matrix dissolves at least at 7% of the less abundant atom. This behaviour qualitatively reproduces the solubility of atoms (e.g. Ti or W) in a-C [11].

3.2.2. Influence of chemical composition.

The influence of chemical composition is of critical importance in this work since it is the parameter that controls the transformation between a polycrystal (composition of 50%) and a nanocomposite (for instance, an overall composition of 25% of A, represents a situation of 50% AB phase together with 50% of pure B phase).

The influence of composition in the number of diffusion events is depicted in Figure 5g. It should be noticed that the simulation with a composition of 0% (only one kind of atom) has the same result than that done with c=0 because in both cases no energetic benefits for crystallization are assigned. In case of the deposit with a composition of 0%, this is a direct consequence of the "DNN rule". It is observed that the number of diffusion events grows when composition increases; this is because GEM-CA has more chances to operate (the composition moves towards a pure crystalline situation), the energy barriers for diffusion are reduced and more diffusion events are possible per deposited atom. In a similar way, the crystalline coverage (Figure 5h) shows a smooth increase from 0% to ca. 90%. In contrast, the behaviour of the grain size is different (see Figure 5i). In fact, the average grain size is quite small (24.5 atoms) up to a composition of 30%, which shows a crystalline coverage of 60%. When the overall composition is changed to 40% there is a sudden jump in the grain size up to ca. 75 atoms, i.e. a factor of 3. The reason for this behaviour is related to the amorphous phase; at a composition of 30%, there is still enough amorphous phase to block the grain growth and embed the grains (ca. 40% of atoms are not crystalline). In contrast, at 40%, the crystalline phase dominates

(only ca. 20% of atoms are not crystalline), and the amorphous phase is actually embedded in the crystalline one. This trend agrees with the results observed for TiC/a-C nanocomposites [11,17], represented by red dots in Figure 5i (note the dedicated right y-axis); thus, the values of TiC grain size remain more or less constant below 5 nm up to 30% of Ti, and then they start growing until values larger than 30 nm at Ti contents close to 50%.

The growth of the average grain size leads to the reduction of the average ratio of external-to-internal crystalline atoms (Fig. 5j), similarly to what occurred in Fig. 5d. The average stoichiometry of the grains is depicted in Fig. 5e. Interestingly, the values remain almost constant at ca. 1.2% up to 30%, in agreement with the behaviour observed for the grain size. Only when the amorphous phase is not dominant, the stoichiometry starts to shift towards unity. Finally, Fig. 5l shows the composition of the amorphous phase. As observed in Fig. 5f, a certain amount of the less abundant atom is always dissolved in the amorphous phase, which can constitute up to its 15% when closer to a stoichiometric film. When the overall stoichiometry is reached, the chemical composition of the amorphous phase becomes stoichiometric as well.

3.2.3. Influence of temperature

Deposition temperature has a major role in KMC since the diffusion probability directly depends on this variable (Eq. 2). The influence of deposition temperature has been previously reported in literature in several structure-zones models (e.g. the Thornton model [18]). Therefore, it is of relevance to study and evaluate the influence of this parameter with the GEM-CA algorithm.

Fig. 5m shows the average number of diffusions per deposited atom. As expected, the variation of temperature from 300 K to 500 K has a dramatic influence on the results (variation of 3 orders of magnitude), much higher than the previous parameters (cf. Figs 5a and 5g). This variation does not produce a significant change in the variation of the crystalline coverage (Fig. 5n), which is more or less constant and high (92-95%). However, when simulating a weaker-forming compound (e.g. using a lower value of c=0.25), the crystalline coverage raises from ca. 50% at 500 K (cf. Fig. 5b) to ca. 75% at 650 K (result not

plotted). In contrast to the crystalline coverage, the average grain size increases with the temperature (Fig. 5o), in agreement with the experimental observations [18]. Nevertheless, the grain growth only becomes noticeable from 400 K on, when it is favoured at expenses of nucleation (the crystalline coverage is almost constant). At 350 K, although there was some 'activation' and the number of diffusions was clearly larger than at lower temperatures (Fig. 5m), the number of diffusions was still too low (around 5) to induce relevant changes in the average grain size. We notice that the grain size and crystalline coverage at low temperatures should be probably lower than the obtained value; this is likely a consequence of the efficiency of GEM-CA, and it will be revisited again in Section 3.3.

The other three parameters under study, the average ratio of external-to-internal crystalline atoms (Fig. 5p), average grain stoichiometry (Fig. 5q) and composition of amorphous phase (Fig. 5r) show similar behaviours than in previous cases (left and central column). The latter two display values in agreement with a composition of 50% (stoichiometry 1 and composition of the amorphous phase around 50%). The former parameter shows a smooth decrease, in agreement with the increase of grain size caused by the increase of the deposition temperature.

3.3. Film growth

In addition to the information described in Section 3.2 (i.e. the influence of simulation parameters in the final structure of the deposit), additional relevant information about the characteristics of the film growth can be obtained from the simulations. To illustrate this possibility, three conditions have been selected (all performed at c=1): i) a composition of 25% with T=500 K (nanocomposite), ii) a composition of 50% with T=500 K (polycrystal) and iii) a composition of 50% with T=300 K (a 'cold' polycrystal). The latter case has been selected to evaluate the influence of a lower number of diffusions in the growth of the film (cf. Fig 5m). Figures 6, 7 and 8 represent the structures of these three scenarios, respectively, at different surface coverage. The three types of representations (deposited atoms, symmetry evaluation and grains) are

included. Figure 9 represents the evolution of several statistical parameters with the surface coverage of the three cases.

Figures 6 and 7 represent the comparison between the growth of a nanocomposite and a polycrystal, respectively; the main difference is not the shape or number of the islands, but the grain size and the amount of amorphous matrix. Thus, Fig. 7 shows a quasi-polycrystalline structure, with large grains and little amorphous phase, while a nanocomposite formed by AB crystals embedded in a B matrix (where some A atoms are dissolved, as indicated before) is shown in Fig. 6. The presence of this second amorphous phase hinders the grain growth in the nanocomposite. This effect has also been reported in the literature [11,15,19], where the presence of an amorphous matrix (e.g. a-C or oxides) keeps the grain size small since it favours the nucleation process at expenses of grain growth. This result opens the possibility of studying the effect of synthesis parameters, such as deposition rate or temperature, on the formation of nanocomposite structures by KMC.

The influence of a lower deposition temperature can be clearly appreciated when comparing the first stages of growth (1%, 20%, 40%) in Figures 7 and 8. At 500 K, the grain growth has clear preference over the nucleation; thus, fewer grain nuclei are observed, which grow with surface coverage. In contrast, at 300 K the number of nuclei is much larger since the diffusion processes are practically forbidden unless they contribute to structures of low energy (e.g. crystals). Therefore, the reason for such unexpected relatively large grain sizes observed at 300 K is probably the diffusion efficiency. In other words, the total number of diffusions is much lower at low temperatures, but *important* diffusions (i.e. those forming crystalline planes) are included among them.

Figure 9 illustrates the evolution of different parameters with the surface coverage of the three cases discussed so far. We have observed that different simulations carried under the same deposition parameters led to similar curves, with much smaller differences than between two different simulation conditions. Nevertheless, in general, simulations carried out with a composition of 50% (central and right column in Fig. 9) show a similar behaviour, the differences being quantitative instead of qualitative; thus, at 500 K there are more internal atoms, less non-crystalline, larger grain sizes and lower number of grains, as it

is expected for a deposit grown at higher temperature. In contrast, the deposit with a composition of 25% is very different; the curves of the number of grains and number of non-crystalline atoms do not reach any steady state. In addition, the amount of crystalline internal atoms is very low, and almost no twins are detected. All these factors are correlated with the control of the amorphous phase, which induces the nucleation of new grains and hiders the grain growth. This fact indicates that the variation of temperature is of minor importance when compared with the influence of chemical composition.

In general terms, the behaviour of the simulations with the surface coverage seems reasonable as expected from experiments. For instance, both nucleation and grain growth take place during almost all the deposition. Notwithstanding, at the end of the simulation, there is a concurrence of observations that indicate possible distortions versus experimental systems: i) The appearance of vacancies is confined at the end of the simulation. ii) Vacancies and growing atoms decrease to zero. iii) Appearance of few triple junctions. iv) Increase of the number of twin atoms. v) Increase of the number of defects. vi) Reaching a steady state in the number of grains (Figs. 9e and h), while the grain size increases (Fig. 9e).

These effects are mainly related to the assumption of a planar lattice (no possibility of atom piling). This limitation has three undesirable effects: (1) the probability of an atom to drop on a grain boundary (or create an antisite defect) instead an empty site of the lattice is dramatically increased (less empty sites available at the end of the deposition). This possibility is almost zero in a real deposition process. As a result, the grain growth could be blocked, because no energetic bonuses are assigned anymore; (2) atoms can be confined to small areas, reducing the possibility of diffusion to reach a stable position; (3) the grains are forced to collide at the end of the simulation, leading to the appearance of twin atoms and false grain growth, due to the collision of two grains with the same orientation. Nevertheless, it is worth mentioning that, in certain situations, events similar to Ostwald ripening [20] have been identified, where a small grain was re-oriented in the direction of a large one close to it. As a consequence of these three limitations, the next development for the GEM-CA algorithm will be the expansion to three dimensions.

4. Conclusions

We have presented here a modified KMC approach to simulate thin film deposition including crystallization processes. To achieve this, a novel crystallization algorithm, named here as GEM-CA, has been introduced into the hopping energy barrier calculation. The problem of "induced order" due to the application of a regular lattice has been successfully avoided by introducing two kinds of atoms in the simulations. The use of two types of atoms had allowed us to obtain both, amorphous and crystalline structures, as a result of the simulations, depending solely on the synthesis parameters. In fact, mixed structures (composites) can be also simulated, opening the possibility of studying their formation by a rather straightforward way, as done with the KMC method used here. Dedicated analysis tools based on the evaluation of symmetry and types of neighbours have been developed for studying the structure of the deposits. The model successfully represents several qualitative experimental observations. However, the planar configuration has been identified as a possible source of distortions, and therefore the upgrade of this model to a 3D level will be carried out in future works.

5. Acknowledgements

The financial support of Portuguese Foundation of Science and Technology (FCT, its acronym in Portuguese), under the project number IF/00671/2013 is gratefully acknowledged. This work has been partially funded by Spanish MCYT FPU program. We are especially grateful to Dr. J.C. Sánchez-López and Dr. A. Fernández for scientific discussions.

6. References

[1] J.M. Albella Martín, Láminas delgadas y recubrimientos: preparación, propiedades y aplicaciones, Consejo Superior de Investigaciones Científicas, Madrid, 2003.

[2] H.N.. Wadley, X. Zhou, R.. Johnson, M. Neurock, Mechanisms, models and methods of vapor deposition, Prog. Mater. Sci. 46 (2001) 329–377. doi:10.1016/S0079-6425(00)00009-8.

[3] P. Bruschi, P. Cagnoni, A. Nannini, Temperature-dependent Monte Carlo simulations of thin metal film growth and percolation, Phys. Rev. B. 55 (1997) 7955–7963. doi:10.1103/PhysRevB.55.7955.

[4] J. Cho, S.G. Terry, R. LeSar, C.G. Levi, A kinetic Monte Carlo simulation of film growth by physical vapor deposition on rotating substrates, Mater. Sci. Eng. A. 391 (2005) 390–401. doi:10.1016/j.msea.2004.09.015.

[5] S.W. Levine, J.R. Engstrom, P. Clancy, A kinetic Monte Carlo study of the growth of Si on Si(100) at varying angles of incident deposition, Surf. Sci. 401 (1998) 112–123. doi:10.1016/S0039-6028(97)00904-7.

[6] P. Zhang, X. Zheng, S. Wu, J. Liu, D. He, Kinetic Monte Carlo simulation of Cu thin film growth, Vacuum. 72 (2004) 405–410. doi:10.1016/j.vacuum.2003.08.013.

[7] D.P. Landau, S. Pal, Y. Shim, Monte Carlo simulations of film growth, Comput. Phys. Commun. 121–122 (1999) 341–346. doi:10.1016/S0010-4655(99)00350-1.

[8] W. Helin, L. Zuli, Y. Kailun, Monte Carlo simulation of thin-film growth on a surface with a triangular lattice, Vacuum. 52 (1999) 435–440. doi:10.1016/S0042-207X(98)00328-5.

[9] M. Breeman, G.T. Barkema, M.H. Langelaar, D.O. Boerma, Computer simulation of metal-on-metal epitaxy, Thin Solid Films. 272 (1996) 195–207. doi:10.1016/0040-6090(95)06946-1.

[10] L. Wang, P. Clancy, Kinetic Monte Carlo simulation of the growth of polycrystalline Cu films, Surf. Sci. 473 (2001) 25–38. doi:10.1016/S0039-6028(00)00941-9.

[11] D. Martinez-Martinez, C. Lopez-Cartes, A. Justo, A. Fernandez, J. Sanchez-Lopez, A. Garcia-Luis, M. Brizuela, J. Onate, Tailored synthesis of TiC/a-C nanocomposite tribological coatings, J. Vac. Sci. Technol. A. 23 (2005) 1732–1736. doi:10.1116/1.210810.

[12] S.W. Levine, P. Clancy, A simple model for the growth of polycrystalline Si using the kinetic Monte Carlo simulation, Model. Simul. Mater. Sci. Eng. 8 (2000) 751–762. doi:10.1088/0965-0393/8/5/308.

[13] P. Bruschi, A. Nannini, M. Piotto, Three-dimensional Monte Carlo simulations of electromigration in polycrystalline thin films, Comput. Mater. Sci. 17 (2000) 299–304. doi:10.1016/S0927-0256(00)00041-0.

[14] N. Ono, K. Kimura, T. Watanabe, Monte Carlo simulation of grain growth with the full spectra of grain orientation and grain boundary energy, Acta Mater. 47 (1999) 1007–1017. doi:10.1016/S1359-6454(98)00391-7.

[15] X. Tan, Y.C. Zhou, X.J. Zheng, Dependence of morphology of pulsed-laser deposited coatings on temperature: a kinetic Monte Carlo simulation, Surf. Coat. Technol. 197 (2005) 288–293. doi:10.1016/j.surfcoat.2004.09.027.

[16] A.F. Voter, Classically exact overlayer dynamics: Diffusion of rhodium clusters on Rh(100), Phys. Rev. B. 34 (1986) 6819–6829. doi:10.1103/PhysRevB.34.6819.

[17] D. Martínez-Martínez, J.C. Sánchez-López, Determination of the thickness of the embedding phase in 0D nanocomposites, Appl. Surf. Sci. 421 (2017) 179–184. doi:10.1016/j.apsusc.2016.12.081.

[18] J.A. Thornton, High Rate Thick Film Growth, Annu. Rev. Mater. Sci. 7 (1977) 239–260. doi:10.1146/annurev.ms.07.080177.001323.

[19] P.. Barna, M. Adamik, Fundamental structure forming phenomena of polycrystalline films and the structure zone models, Thin Solid Films. 317 (1998) 27–33. doi:10.1016/S0040-6090(97)00503-8.

[20] T. Tadros, Ostwald Ripening, in: T. Tadros (Ed.), Encycl. Colloid Interface Sci., Springer Berlin Heidelberg, Berlin, Heidelberg, 2013: pp. 820–820. http://link.springer.com/10.1007/978-3-642-20665-8_124 (accessed November 6, 2017).

7. Tables

Table 1. Parameters used in this work.

Distances (atomic units)			Energies (eV)							Constants
$r_0=r_{NN}$	r_{NNN1}	r_{NNN2}	E_S	E_D	E_L	V_0	E_{NN}	E_{NNN1}	E_{NNN2}	a
1	$\sqrt{3}$	2	0,75	0,25	0,15	0,35	-0,35	-0,11	-0,06	2,47

Table 2. Base input variables used in the simulations. Highlighted in **bold** are indicated the values set constant when any other parameter was varied.

Lattice Size (atoms)	Number of substrate defects	Deposition rate (monolayers/sec)	Deposition time (sec)	T (K)	Composition	c
100×100	0	0,0025	400	200-**500**	0-**50**%	0-**1**-3

Table 3. Types of atomic positions according to the symmetry and type of NN's.

Label	Description	Color for representation
Crystalline internal	Atom surrounded by 6 atoms, 2 of its same kind in opposed positions, and 4 different in the other positions. The NN atoms must be crystalline as well, internal or external.	Blue
Crystalline external	Atom similar to the internal, but at least one of the atoms in NN is not crystalline.	Red
Boundary	Atom in NN to a crystalline external that it is not crystalline (internal or external).	Yellow
Twin	Boundary atom belonging to two grains	Green
Triple juncture	Boundary atom belonging to three grains	Pink
Growing	Atoms that are in NN to a boundary atom (or another growing), with good symmetry for grain growth, but with at least one empty NN.	Dark golden
Antisite defect	Atom of type A located in a place where an atom of type B was expected, or vice-versa. It is surrounded by boundary atoms.	Purple
Vacancy	Similar to the antisite defect, but characterized by an empty position instead an atom of the wrong type.	Magenta
Amorphous	Any atom not belonging to any of the previous classes.	Grey

8. Figure Captions:

Figure 1. High-resolution transmission electron images of thin films composed by Ti and C. a) Polycrystalline TiC. b) Nanocomposite formed by small TiC grains surrounded by an a-C matrix. [11]

Figure 2. a) Possible values of parameter β depending on the diffusion obstacles. b) Type of neighbours in a hexagonal lattice considered in this model.

Figure 3. Operation of the crystallization algorithm GEM-CA. a) Geometry arrangements in which a central atom A type gives energy bonuses to its NN. The values of the bonuses have the opposite sign if the central atom is B type. Geometrical configurations symmetrically equivalent to the represented ones are also awarded (an expanded version of this figure is included in the supplementary material). b and c) Example of the influence of GEM-CA in the energy barrier E_B on two diffusions reaching a position with the same number of neighbours. In (c) E_B is lower than in (b) because the position of arrival has 3 ordered NN which gives extra stabilization to a B atom (P=-3). d to f). Effect of the application of the "DNN rule" in the growth of crystal planes. The values of the P parameter are shown considering the atoms depicted. d) Situation before diffusion. e) When DNN is deactivated, the A plane (in red) gives stabilization and can continue growing without the need of the rest of crystal to grow. f) When DNN is activated, a B atom has to be in NN position to give bonuses.

Figure 4. Influence of the GEM algorithm in the crystallization of films deposited at 500 K with a composition of 50%, observed at surface coverages of 50% (a, c) and 100% (b, d). a, b) GEM disconnected (c=0). c, d) GEM connected (c=1). The colour of the atoms in the images of the first column represents the nature of each atom (A or B). In the second column, the colour represents the type of atom according to the symmetry and type of the surrounding atoms (see Table 3). In the third column, the different grains are highlighted. Positions classified as 'boundary', 'twin', 'triple junction', 'defect' or 'vacancy' are also represented with the same colour code than in the second column. Movies showing the

growth of these films with the three types of representation are included as supplementary material.

Figure 5. Influence of simulation conditions in different parameters of the deposit: number of diffusions per deposited atom (*a, g, m*); coverage of crystalline atoms (*b, h, n*); average grain size (*c*, *i*, *o*); average ratio between crystalline external and crystalline internal atoms (*d, j, p*); average stoichiometry of the grains (*e, k, q*); chemical composition of the amorphous phase (*f, l, r*). Left column: influence of parameter *c*, for two compositions (50%, in red, and 25% in black). Center: influence of composition. Right: influence of deposition temperature. In some cases, fitting functions have been used to represent the overall trends; the lines in *e*, *g*, *n*, *p*, *q* and *r* are linear fittings; curves in *j* and *k* are parabolic fittings; a polynomic function of order 3 was used in *h*, and exponentials were used in *b* (Eq. 8). Experimental points for TiC/a-C nanocomposites [11,17] are included in *i*, where the right Y-axis varies between 0 and 70 nm. Images of the grains at complete surface coverage are included for extremal values of the parameters under study. Movies showing the growth of these films with the three types of representation are included as supplementary material.

Figure 6. The growth of a film of 25% composition at 500K. Top row: deposited atoms. Central row: the analysis based on the symmetry and types of the NN positions to each atom (see Table 3). Bottom row: formed grains. Movies showing the growth of this film with the three types of representation are included as supplementary material.

Figure 7. The growth of a film of 50% composition at 500K. Top row: deposited atoms. Central row: the analysis based on the symmetry and types of the NN positions to each atom (see Table 3). Bottom row: formed grains. Movies showing the growth of this film with the three types of representation are included as supplementary material.

Figure 8. The growth of a film of 50% composition at 300K. Top row: deposited atoms. Central row: the analysis based on the symmetry and types of the NN

positions to each atom (see Table 3). Bottom row: formed grains. Movies showing the growth of this film with the three types of representation are included as supplementary material.

Figure 9. Evolution of different statistical parameters during the growth of three films deposited at different conditions. Left column (a to c): composition 25%, temperature 500 K. Central column (d to f): composition 50%, temperature 500 K. Right column (g to i): composition 50%, temperature 300 K.

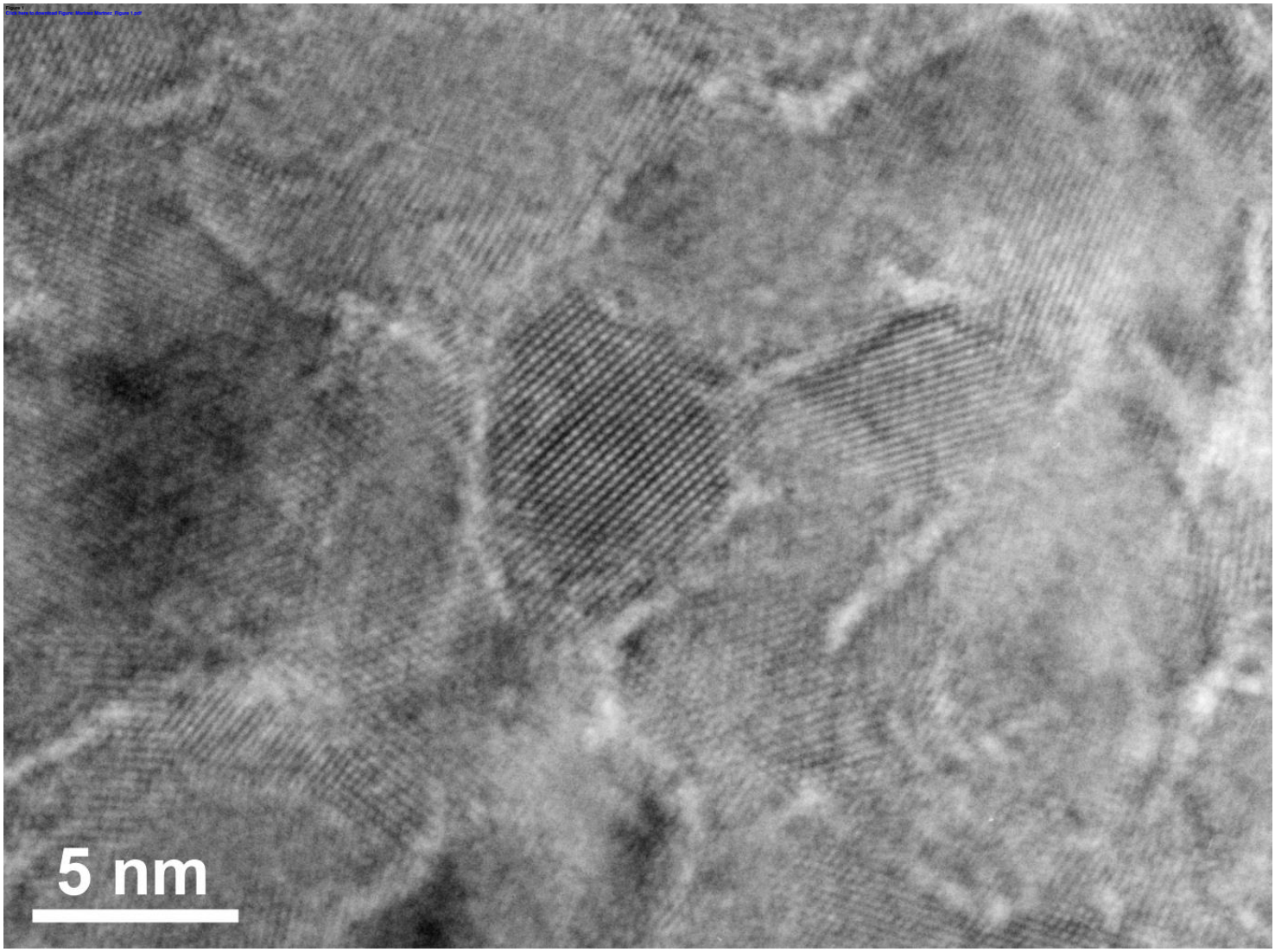
5 nm

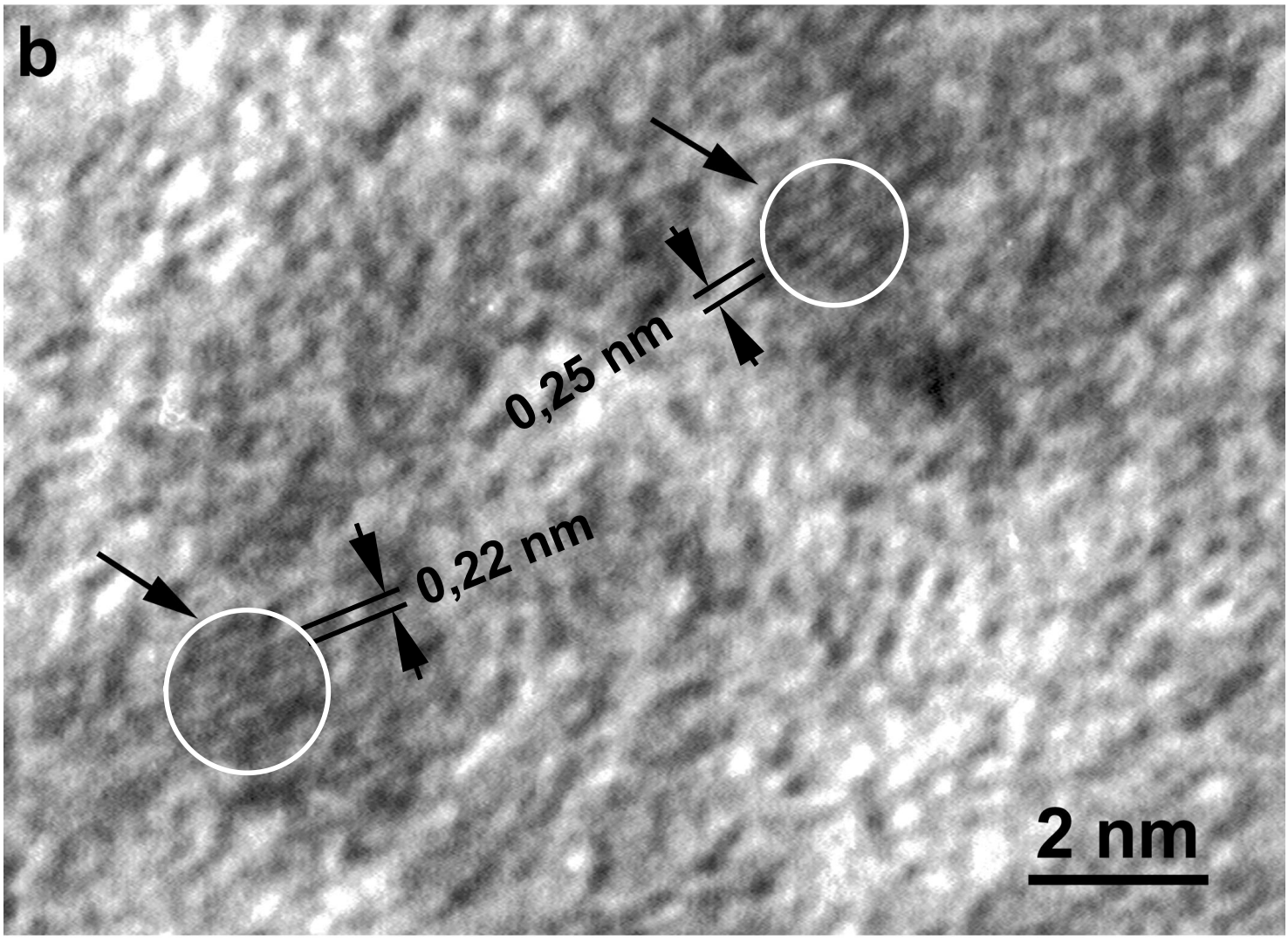
b
0,25 nm
0,22 nm
2 nm

Figure 2

Click here to download Figure: Martnez Martnez_Figure 2.pdf

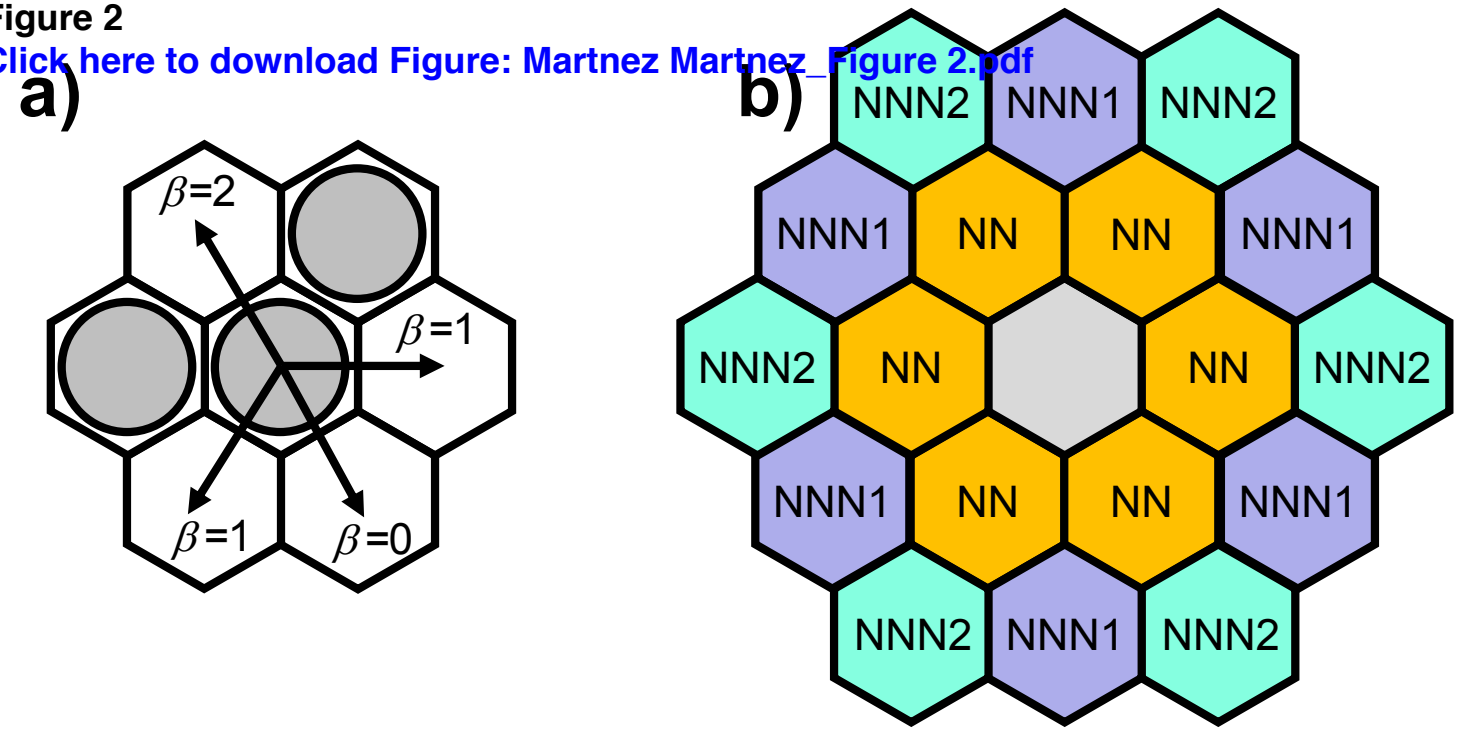

Figure 3

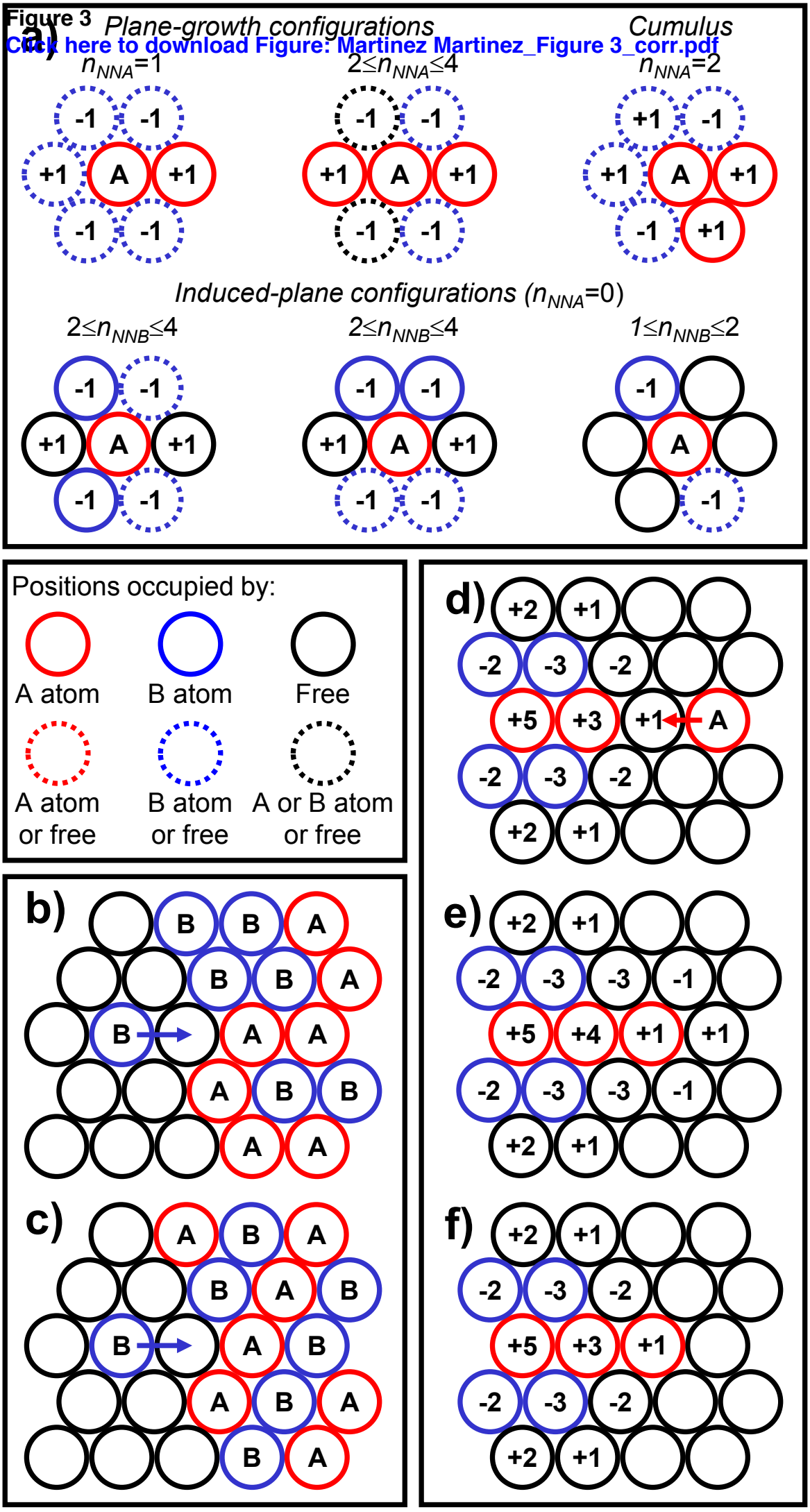

Figure 4
Click here to download Figure: Martinez Martinez_Figure 4.pdf

a)

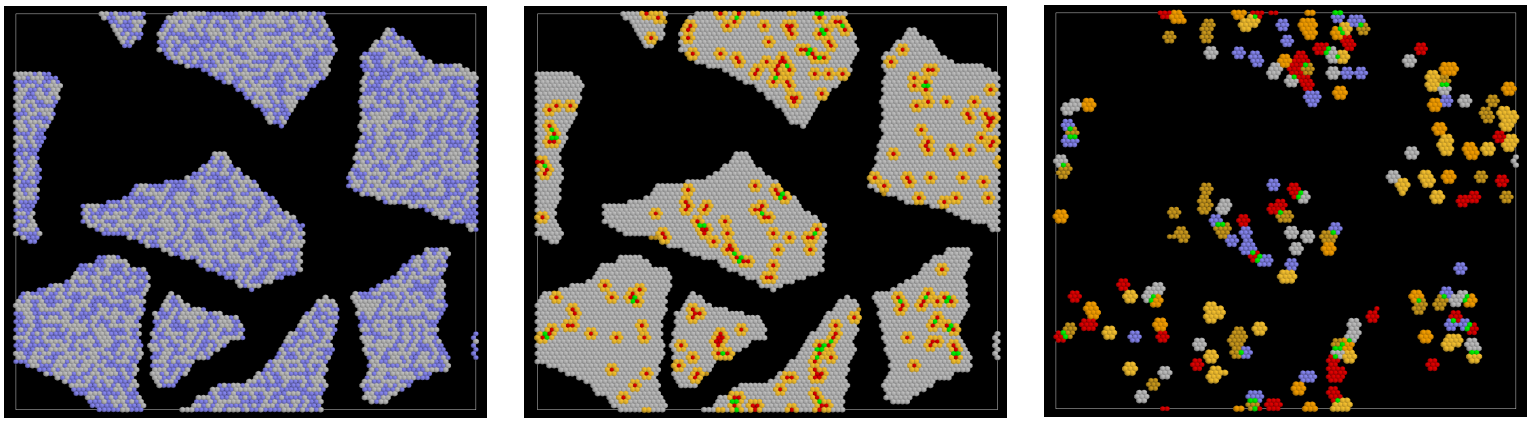

b)

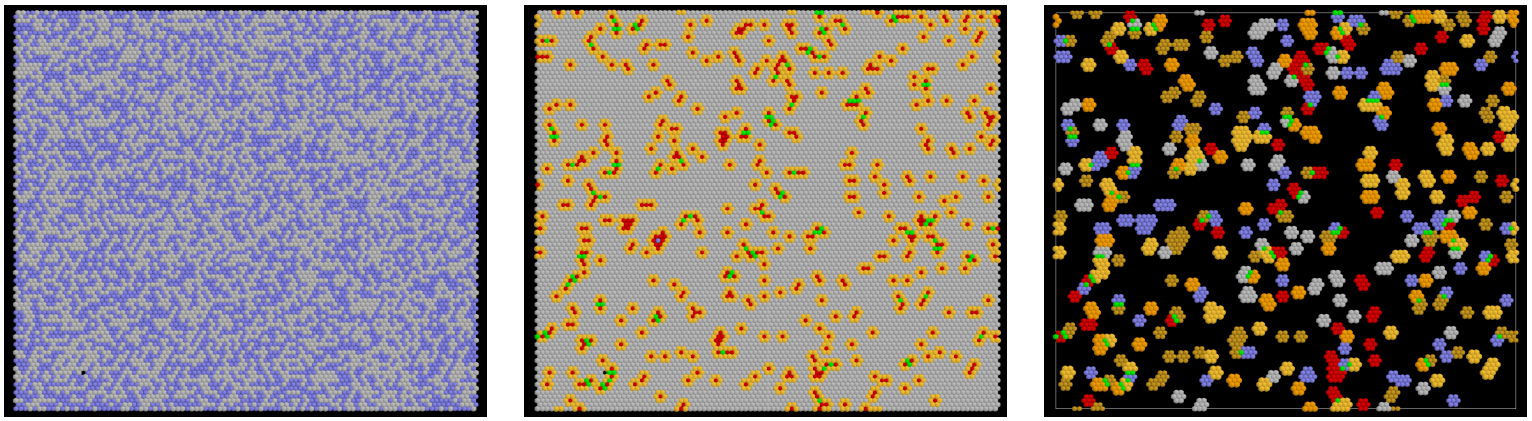

c)

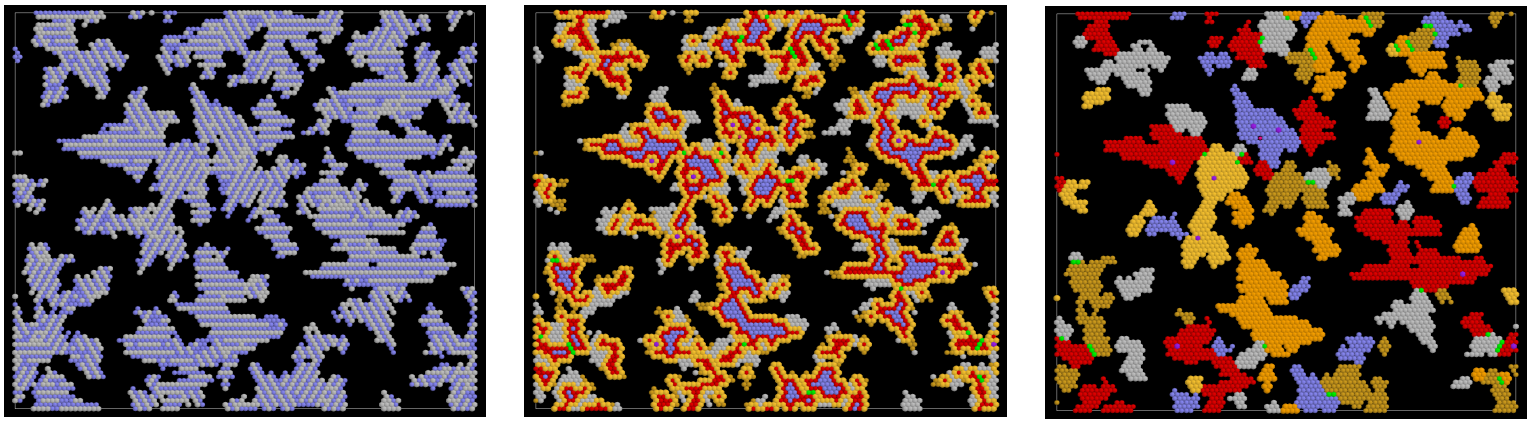

d)

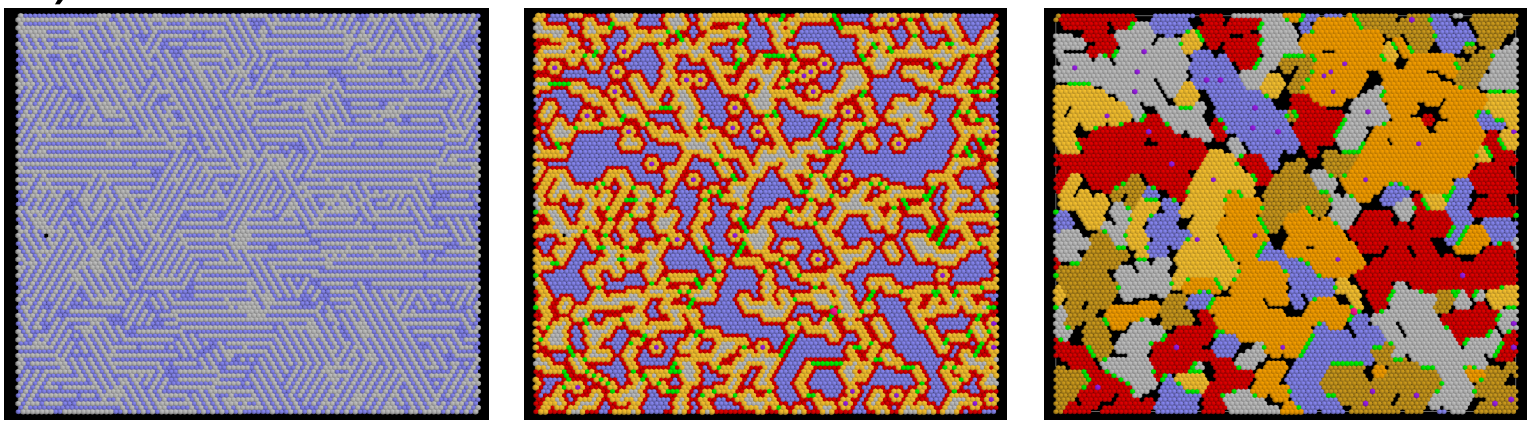

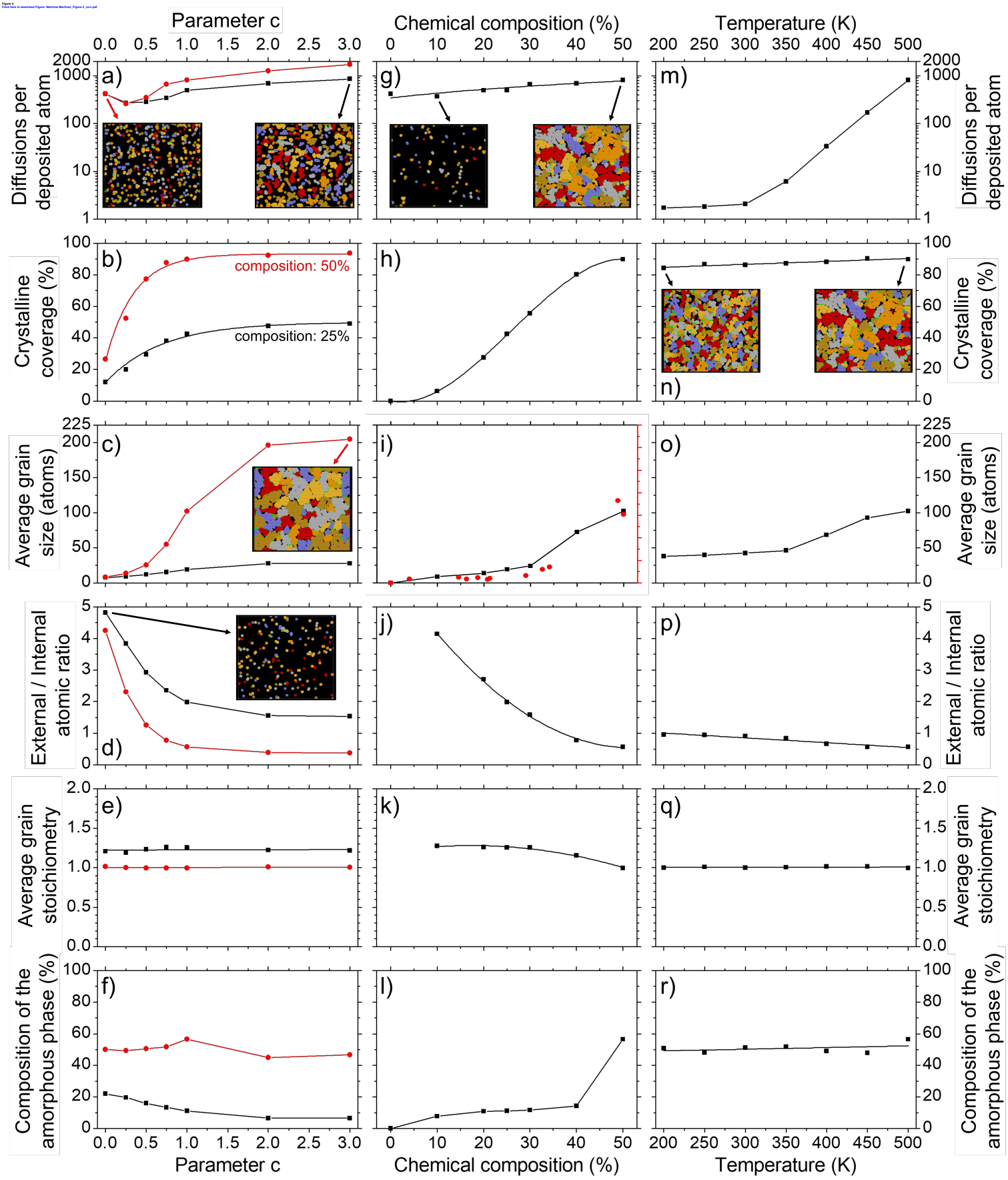
Parameter c
Chemical composition (%)
Temperature (K)
Diffusions per deposited atom
Crystalline coverage (%)
Average grain size (atoms)
External / Internal atomic ratio
Average grain stoichiometry
Composition of the amorphous phase (%)
a)
b)
c)
d)
e)
f)
g)
h)
i)
j)
k)
l)
m)
n)
o)
p)
q)
r)
composition: 50%
composition: 25%

Figure 6
Click here to download Figure: Martinez Martinez_Figure 6.pdf

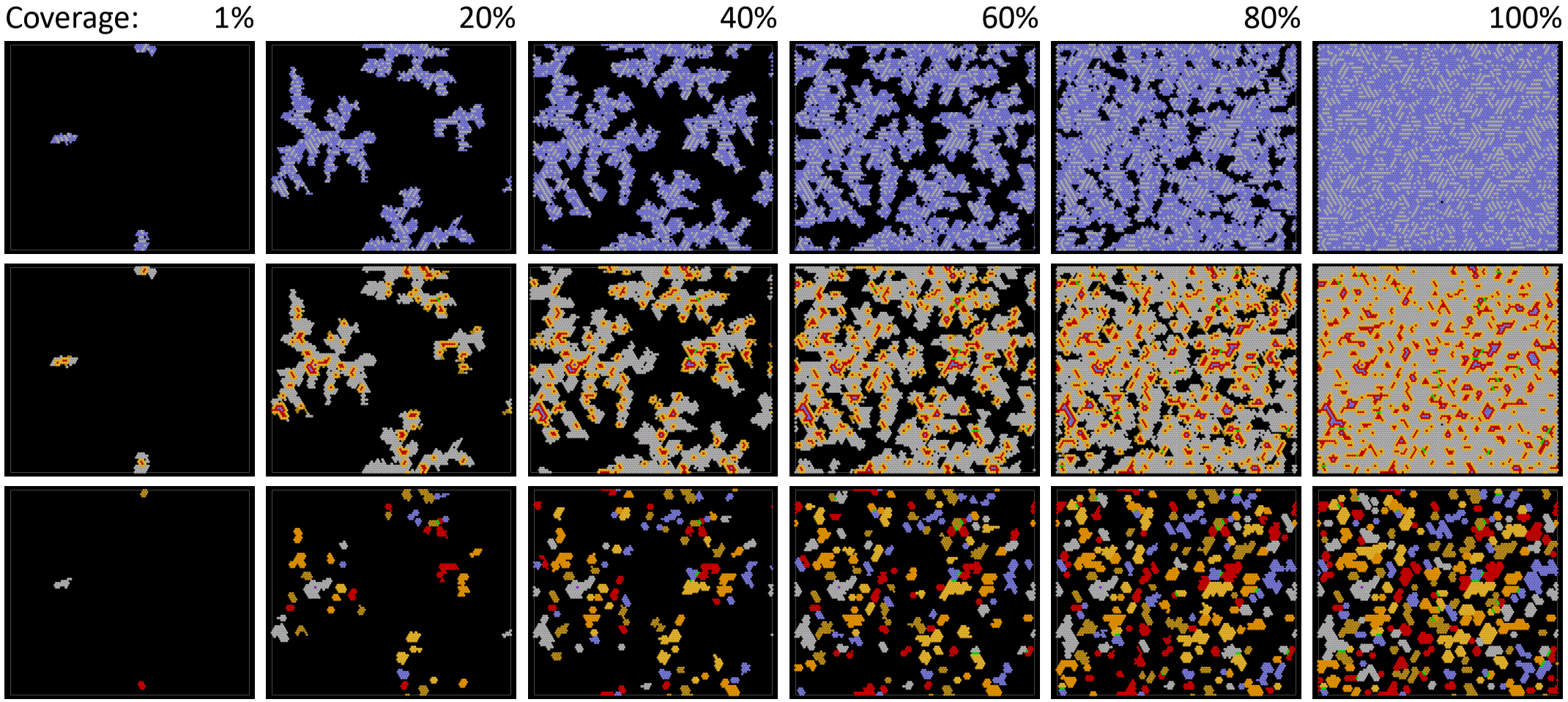

Figure 7
Click here to download Figure: Martinez Martinez_Figure 7.pdf

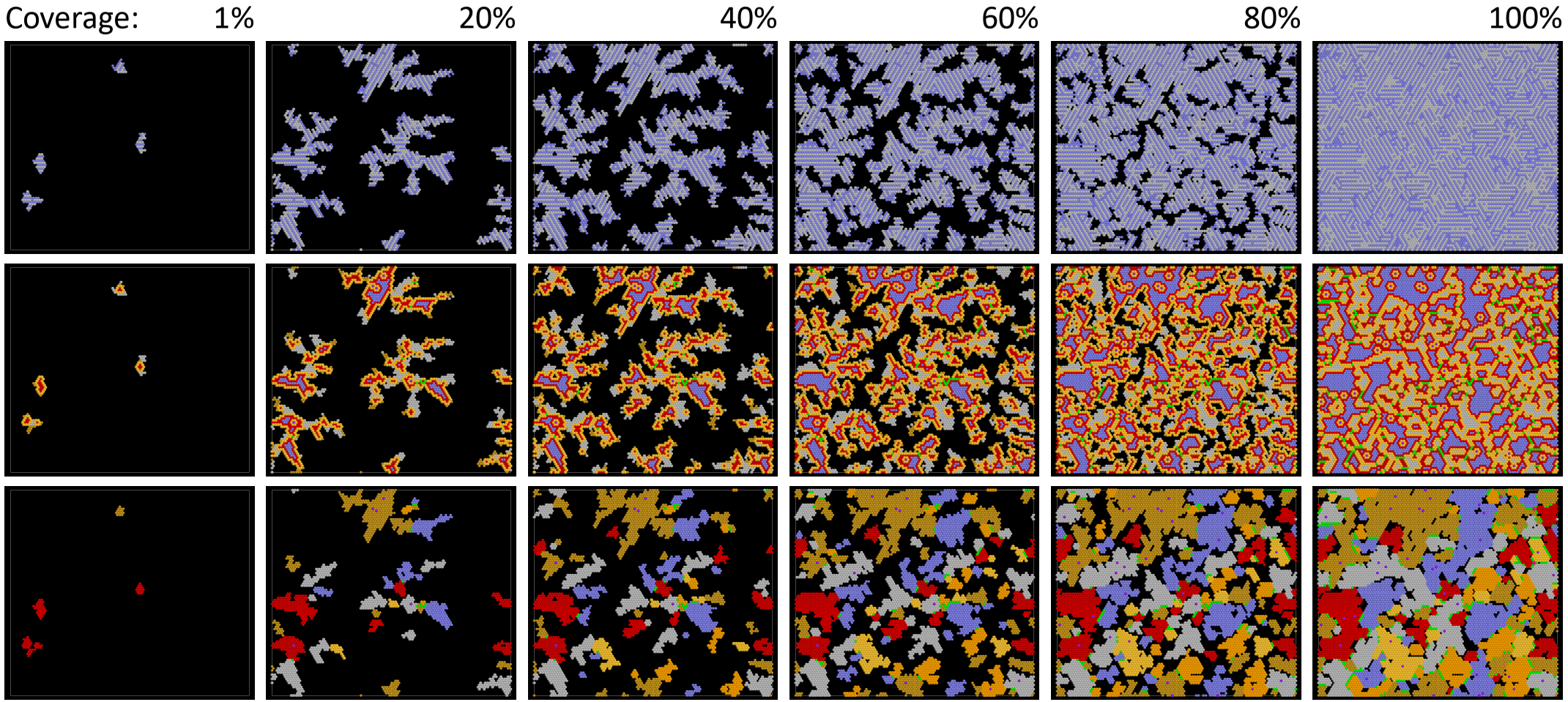

Figure 6
Click here to download Figure: Martinez Martinez_Figure 6.pdf

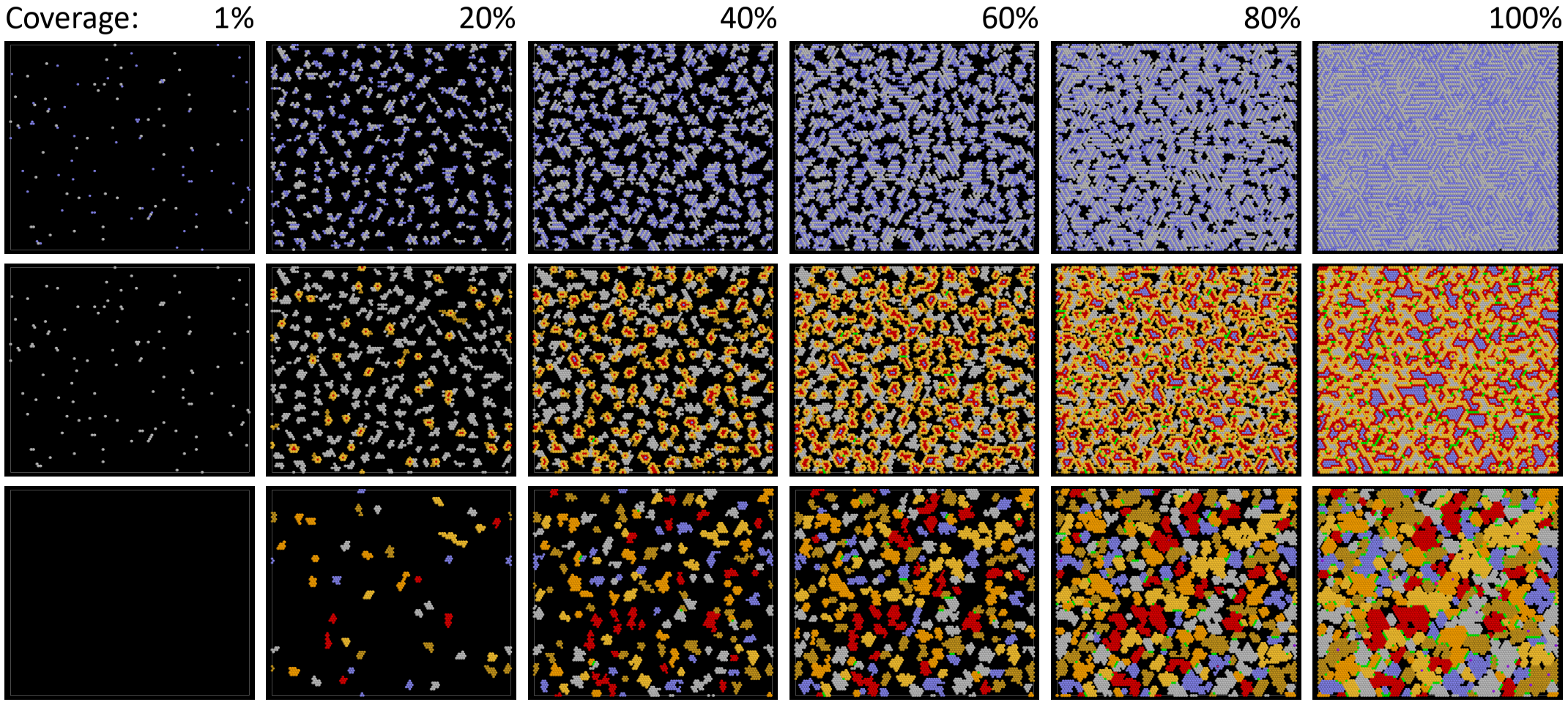

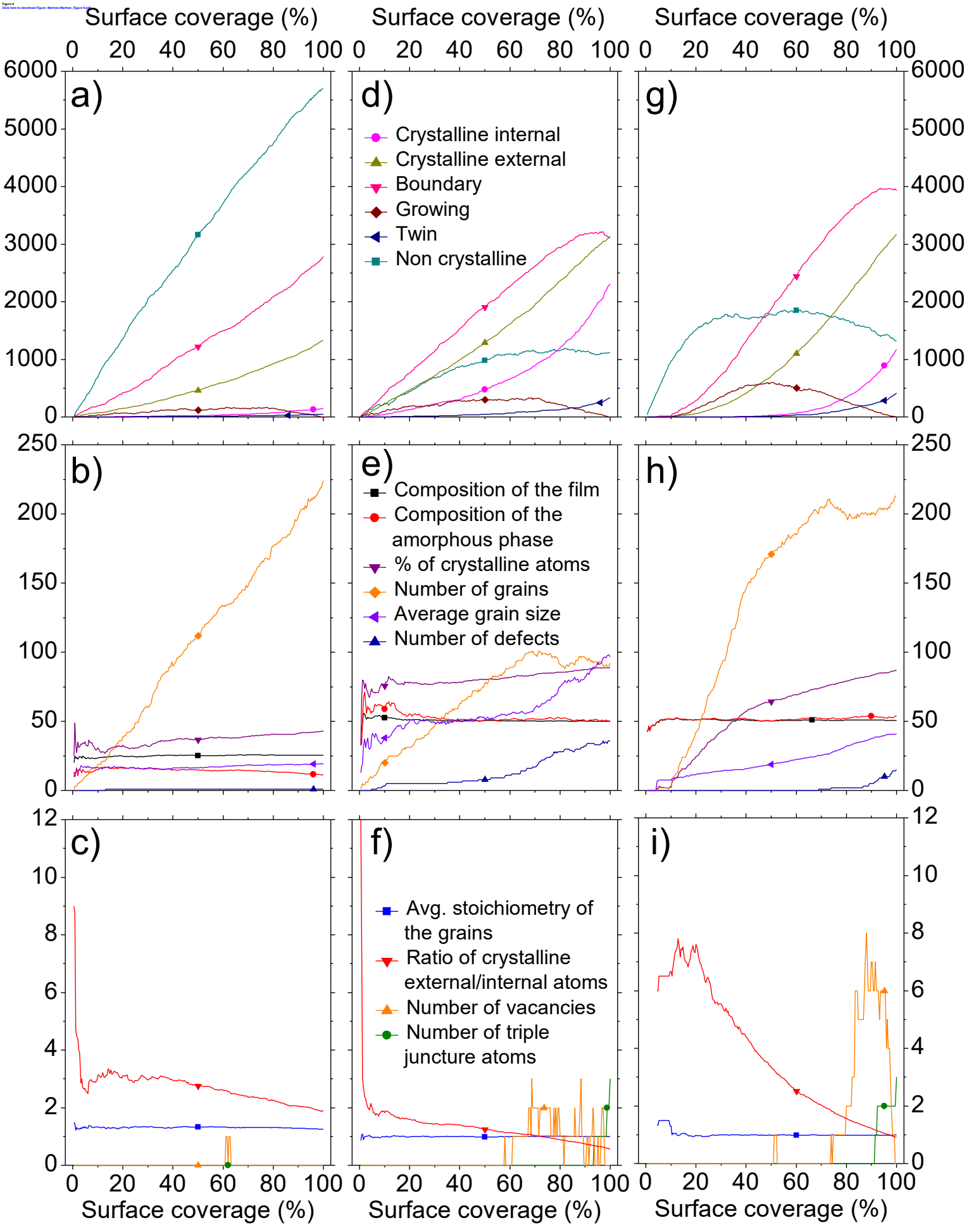
a)
b)
c)
d)
e)
f)
g)
h)
i)
Surface coverage (%)
Crystalline internal
Crystalline external
Boundary
Growing
Twin
Non crystalline
Composition of the film
Composition of the amorphous phase
% of crystalline atoms
Number of grains
Average grain size
Number of defects
Avg. stoichiometry of the grains
Ratio of crystalline external/internal atoms
Number of vacancies
Number of triple juncture atoms